Atomization and Sprays, vol. 6, pp. 285-304, 1996

COMPARATIVE STUDY OF TWIN-FLUID ATOMIZATION USING SONIC OR SUPERSONIC GAS JETS

B. K. Park and J. S. Lee
Department of Mechanical Engineering, Seoul National University, Seoul, Korea

K. D. Kihm
Department of Mechanical Engineering, Texas A & M University, College Station, Texas, USA

To examine the effect of sonic and supersonic gas jets on twin fluid atomization, a comparative study has been done for two different types of atomizers, using (1) an underexpanded sonic nitrogen gas jet from a converging nozzle (SN type), and (2) an overexpanded supersonic nitrogen gas jet from a converging-diverging nozzle (CD type, with an area ratio of 3). Water is used as the atomized liquid injected through a center orifice. The Malvern diffraction sizer measured the spray Sauter mean diameter (SMD) distributions on a line-of-sight basis and a tomographic transforma tion of the data found the radial distribution of drop SMDs. A Buckingham-PI dimensional analysis provided an experimentalcorrelation of the spray SMD with the radial and axial location, liquid mass flux, and the gas jet stagnation pressure. The SMD correlation showed small distinctions (approximately 7.5%) between the two different nozzle types when other injection conditions remained fixed. The stagnation pressure showed a dominance over the nozzle configuration (SN or CD type) in determining atomization. Also, a modified energy model analysis provided a single correlation for spatially averaged SMDs for both SN- and CD-type nozzles. The stagnation pressure again played a dominant role when correlating the spatially averaged drop SMDs.

INTRODUCTION

Liquid atomization in high-speed gas environments is important in many industrial processes, for example, supersonic combustion for gas turbines, spray drying and cooling, liquid metal atomization, and spray painting. High-pressure gas injection can develop subsonic, sonic, or supersonic jets, depending on the nozzle configuration and the range of stagnation pressure. For a specified range of stagnation pressure after the nozzle is choked, a converging nozzle develops underexpanded sonic jets with Prandtl-Meyer expansion fans established at the nozzle exit (Fig. 1). However, converging-diverging nozzles can develop overexpanded supersonic jets with oblique shocks attached to the nozzle exit for the same range of the stagnation pressure. Because of these distinctive features of the expansion and shock waves of the gas jets, different nozzle configurations can result in different atomization characteristics.

Questions to ask are: "Which nozzle configuration between converging and converging-diverging gives better atomization efficiencies generating smaller drops under a

The authors would like to acknowledge Dr. Lee G. Dodge of the Southwest Research Institute, San Antonio, Texas, for his generous provision of the tomographic deconvolution software ONION, which was originally developed by Prof. Rolf D. Reitz, University of Wisconsin, and Dr. Lee G. Dodge. This work was supported by the Korea Ministry of Education through the Mechanical Engineering Research Fund (ME 93-A-08).

NOMENCLATURE

A_e	nozzle exit area, m^2	SMD	Sauter mean diameter, μm
A^*	nozzle throat area, m^2	T	temperature, K
ALR	air-to-liquid mass flow rate ratio	U	flow velocity, m/s
AR	nozzle exit-to-throat area ratio	We_{d_0}	Weber number based on d_0 $\left(\mathrm{We}_{d_0} \equiv \frac{\rho_L U_R^2 d_0}{\sigma}\right)$
d_0	diameter of liquid delivery tube, mm	x	axial distance, mm
D	drop diameter, μm	γ	specific heat ratio
GLR	gas-to-liquid mass flow rate ratio	ε	energy transfer efficiency, Eq. (13) or Eq. (15)
I	impulse function, Eq. (2)	μ	dynamic viscosity, Pa s
$\dot{m}$	mass flow rate, kg/s	ρ	density, kg/m^3
M	Mach number	σ	surface tension, N/m
p_b	backpressure, MPa		
p_t	stagnation or nozzle injection pressure, MPa		**Subscripts**
R	specific gas constant, J/kg K		
$\Re_I$	impulse function ratio of SN-type to CD-type nozzle, Eq. (4)	e	nozzle exit
		G	gas
r	radial distance, mm	L	liquid

given stagnation condition?" or "Is there a dominant parameter deciding the atomization and overriding the geometrical effect of different nozzle configurations?" To the authors' knowledge, these questions have not been answered. The authors have done a series of investigations to explore and answer these proposed questions.

For relatively low-sped gas atomization, several works have investigated the average drop size distribution in terms of related parameters [1-4]. Generally accepted findings are that the drop size increases with an increase in liquid viscosity and surface tension, but decreases with increasing gas/liquid mass ratio, liquid density, and gas velocity. Quantitative and systematic studies of high-speed gas atomization have not been done as much. The difficulty in experimentally controlling the sonic or supersonic flows and complexity in their theoretical analyses have limited the study of high-speed atomization in the compressible flow range (M > 0.35).

Hanson et al. [5] studied the breakup mechanism in a shock tube for various liquid droplets that were levitated using acoustic waves. They used photography to study the shattering of a stationary drop when a normal shock runs over it. The critical Weber numbers where the droplet breaks into smaller ones were examined extensively in the study.

Ranger and Nicholls [6, 7] visualized the breakup process with shadowgraphic photographs. They observed the interactions of drops ranging from 750 to 4000 μm in diameter and for a Mach number range from 1.5 to 3.5. High-speed convective flow played a dominant role in the breakup process. The breakup time scale was proportional to drop diameter but inversely proportional to air velocity.

Schetz et al. [8] documented photographically the spray development of Freon-12 cross-injected into a free-stream Mach number of 0.44. They showed that the evaporation must be included, especially for the study of chilled fluid injected into a hot environment. Unal [9] visualized the flow in a supersonic atomization nozzle and obtained the drop size distribution for an aluminum alloy.

Kihm and Chigier [10] measured the drop size distributions using a laser diffraction technique to investigate the effect of shock waves on the atomization using a two-dimensional

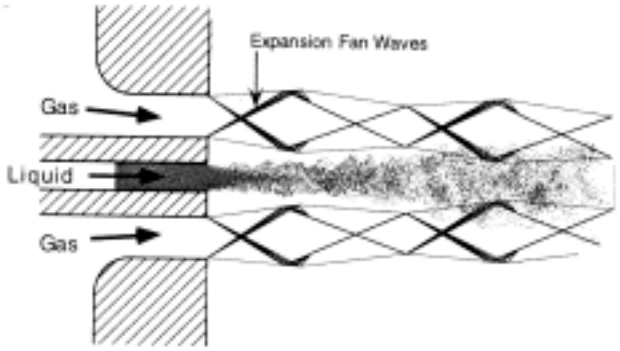

(a) Underexpanded sonic jet from the SN-Type nozzle

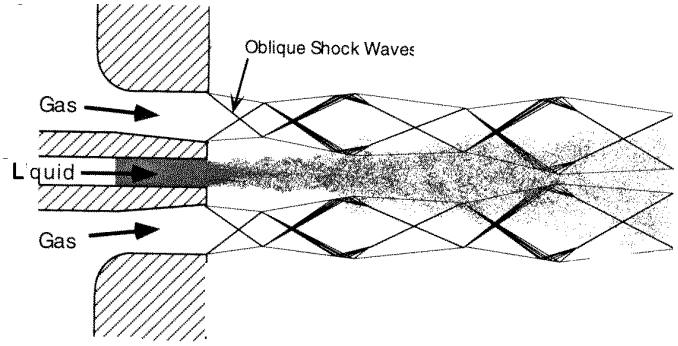

(b) Overexpanded supersonic jet from the CD-Type nozzle

Fig. 1 Twin-fluid atomizations by two different gas jets: (a) underexpanded sonic gas jets from a concentric converging nozzle; (b) overexpanded supersonic gas jets from a converging-diverging nozzle.

plane sonic nozzle. They observed that the drop Sauter mean diameters (SMDs) decreased with increasing air/liquid mass ratio and with increasing air velocity weighted by its local density, i.e., the air mass flux. They postulated that an atomization limit below the critical Weber number was already reached before the sonic condition and the further development of shock waves did not significantly influence the atomization.

The present article summarizes the findings in comparing atomization by under-expanded sonic gas jets and then by overexpanded supersonic gas jets. The tested twin-fluid atomizers injected water as the atomized liquid through the center orifice. The wellestablished diffraction method (the Malvern technique) measured the "line-of-sight" distributions of drop SMDs. Tomographical transformation of the data provided spatially

resolved drop SMDs [11, 12]. Buckingham-PI dimensional analysis correlated the drop SMD data in terms of the radial and axial coordinates and other dimensionless parameters. An energy model, originally developed and used for two-dimensional plane nozzles [13, 14], has been modified to analyze the spatially averaged SMD data for the present axisymmetric sprays.

EXPERIMENTS

Tested Nozzles and Rigs

Two different types of concentric gas nozzles were studied. One was a sonic converging nozzle (SN-type nozzle, Fig. 1*a*) that gave underexpanded sonic jets and successfully developed the repeated patterns consisting of expansion waves and oblique shock waves in order. The other was a supersonic converging-diverging nozzle (CD-type nozzle, Fig. 1*b*) that provided overexpanded supersonic jets, which were followed by the repeated patterns of oblique shock waves and expansion waves. The underexpanded jet exhausts sonic flow of M = 1.0 and the overexpanded jet exhausts supersonic flow. On the other hand, the underexpanded jet provides higher exit pressure than the overexpanded jet, which generates an exit pressure lower than the ambiant. The nozzle exit temperature decreases significantly with increasing Mach number. In addition to these differences in jet properties, the initial shear patterns are different between the two nozzles. For the SN-type nozzle the liquid first interacts with the series of expansion fan waves of the underexpanded and choked sonic flow, and for the CD-type nozzle the first interaction of liquid is made with the oblique shock waves of the overexpanded supersonic flow.

Figure 2 shows a schematic arrangement of the experimental apparatus. A high-speed gas jet is generated by evaporating liquid nitrogen. The liquid nitrogen, pressurized by a pressure-building regulator and a pressure-building valve, enters the evaporator through the liquid valve. The evaporated liquid nitrogen, with its pressure adjusted by the pressure regulator, is supplied to the nozzle through the solenoid valve. The nitrogen gas flow rate is found from the measured stagnation pressure of supplied gas assuming isentropic flow. A constant flow rate is confirmed by the analog signals obtained from the pressure transducer installed at the nozzle wall. The water flow rate through the central orifice is controlled independently by both a variable flow meter and a rotameter.

Figure 3 shows detailed configurations and dimensions of the two different twin-fluid atomization nozzles. The liquid is supplied through the liquid delivery tube in the center and the pressurized gas is injected through an annular jet. The inner wall of the gas flow passage has two different shapes: a straight type (SN-type nozzle) for underexpanded sonic jet development and a tapered type (CD-type nozzle) for overexpanded supersonic jet. The throat areas of both nozzles are 9.14 mm^2. Both nozzles satisfy the symmetry of the spray development and its ensemble-averaged SMD distribution within approximately 5% consistency.

Table 1 summarizes the experimental conditions. The area ratios of the throat to exit were 1.0 for the SN-type and 3.0 for the CD-type nozzle. The two nozzles require 0.192 MPa and 2.15 MPa stagnation pressure, respectively, to achieve isentropic expansion without resulting in Prandtl-Meyer expansion fans or oblique shock waves at the nozzle exit. Corresponding nozzle exit Mach numbers are 1.0 and 2.64, respectively. For the tested stagnation pressure range of 0.2 MPa $\leq p <$ 0.5 MPa, the SN-type nozzle establishes

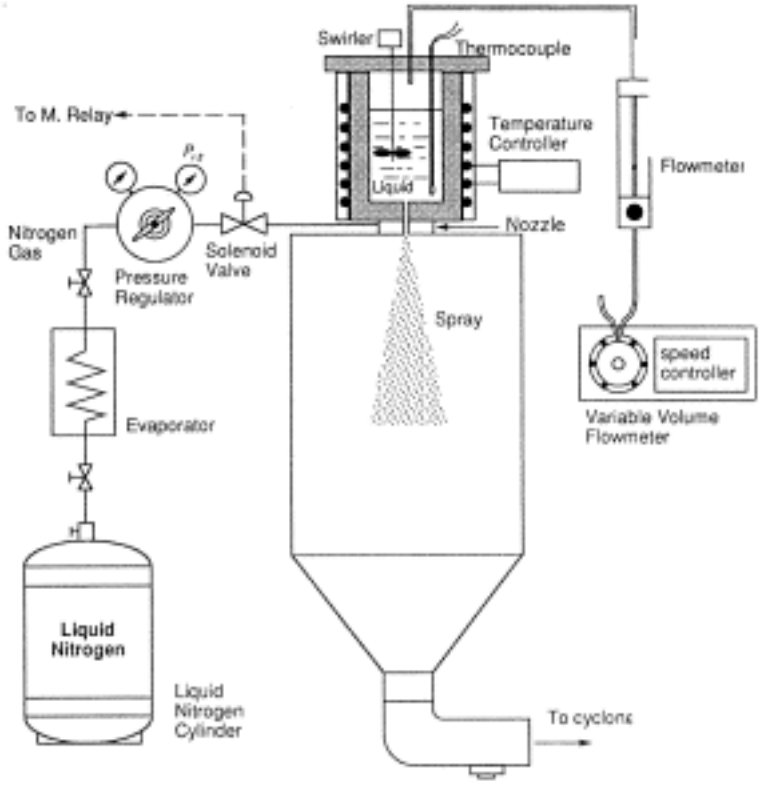

Fig. 2 Schematic of experimental apparatus.

underexpanded sonic jets, and for the range of 0.25 MPa ≤ p_t ≤ 0.4 MPa, the CD-type nozzle develops overexpanded supersonic jets. Since both nozzles are choked for the entire range of tested stagnation pressures, the mass flow rate is determined solely by the stagnation conditions, regardless of the nozzle type.

A pressure transducer (Validyne DP 15 TL, CD 12 transducer indicator) and Burdon gauge connected to a pressure tap drilled at the side of the nozzle chamber measured the stagnation pressure. The pressure was converted to an analog signal calibrated with a range from 0 to ± 1 V in the pressure transducer indicator, then converted to a digital signal in an integrating voltmeter module (HP 44701) of the data acquisition system (HP 3852A) and sent to a personal computer. The personal computer made an average of 100 measurements and selected data with maximum variations within ± 0.03%.

Impulse Function of SN-Type and CD-Type Nozzles

Beyond the choking, the mass flow rate for both SN-type and CD-type nozzles is expressed in terms of the stagnation properties as [15]

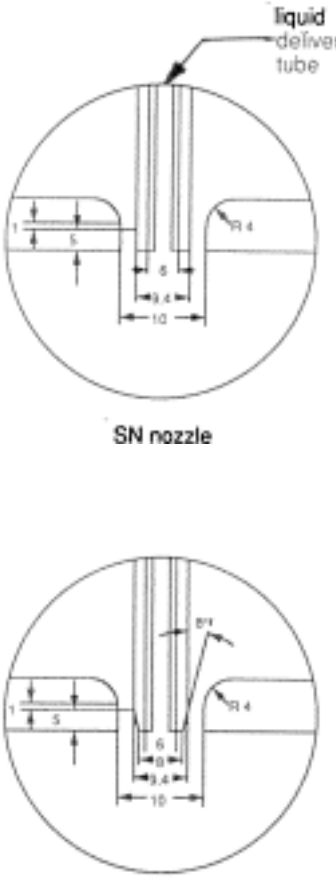

Fig. 3 Cross-sectional views of the tested twin-fluid atomization nozzles.

$$\dot{m}_G = \frac{p_t}{\sqrt{RT}} A^* \sqrt{\gamma} \left(\qquad ^{(\gamma+1)/(2-2\gamma)} \qquad (1$$

The mass flow rate depends only on stagnation pressure and temperature when the nozzles are choked with the same throat area, regardless of the nozzle type. Applying the momentum equation to a control volume surrounding a rocket nozzle, the jet thrust or impulse function, 1, is given by [16]

$$\text{Thrust} = I = \dot{m}_G U_e + (p_e - p_b) A_e \qquad (2)$$

where p_e denotes the nozzle exit pressure and p_b indicates the ambient or back pressure (101.3 kPa for the present case). The nozzle exit area $A_e = A^*$ for the SN-type nozzle and $A_e = 3.0\ A^*$ for the CD-type nozzle. V_e and p_e, can also be expressed in terms of the stagnation pressure and temperature from isentropic flow relationships.

Substitution of Eq. (1) into Eq. (2), with proper conversions of Ve and pe in terms of p_t, and T_t gives a reduced expression for the impulse function as

$$I = A^* p_b \left[\text{Const} \left(\frac{p_t}{p_b} \right) - \text{AR} \right] \qquad (3)$$

where the Const is calculated as 1.2680 for the SN-type nozzle with a nozzle exit-to-throat ratio AR of 1.0, and as 1.5267 for the CD-type nozzle with AR = 3.0.

In twin-fluid atomization applications, both the jet momentum and pressure differential force contribute to the shear action to break up the liquid column. Thus, it is expected that the impulse function, which consists of the jet momentum and pressure contributions [Eq. (2)], could be a measure of the atomization performances. The ratio of SN-nozzle impulse function with AR = 1.0 to CD-nozzle impulse function with AR = 3.0 is given as

$$\Re_I = \frac{I_{SN}}{I_{CD}} = \frac{(1.2680 \cdot p_t/p_b - 1.0)}{} \qquad (4)$$

Note that the impulse ratio, $\aleph$, depends only on the ratio of stagnation to back pressure when the two nozzles have identical throat areas.

Figure 4 shows the impulse ratio $\Re_I$, versus p_t/p_b. For p_t/p_b less than the critical value of 7.731 corresponding to $\Re_I = 1.0$, the impulse function of the SN-type nozzle is higher

Table 1 Summary of Experimental Parameters

Tested nozzles	Converging sonic nozzle (SN type) and Converging-diverging supersonic nozzle (CD type)
Nozzle throat area A^* (mm^2)	
Exit-to-throat area ratio AR	1.0 for SN type 3.0 for CD type
Nozzle injection pressure or stagnation pressure p_t (MPa)	0.2, 0.25, 0.3, 0.4, 0.5 for SN type 0.25, 0.3, 0.4 for CD type
Liquid orifice diameter d_0 (mm)	4.0
Liquid flow rate, Q (ml/min)	100, 200, 300
x (mm)	70, 160
r (mm)	0 to 55
Ratio of jet inertia to viscous force [Eq. (14)]	Ranging from 50 to 350
Size distribution model for Malvern data analysis	Rosin-Rammler two-parameter model

than that of the CD-type nozzle. For p_t/p_b larger than 7.731, the CD-nozzle impulse function is larger than that for the SN-nozzle and the ratio approaches an asymptotic value of 0.831 as p_t, increases further. For the present study's tested range of ON from 1.97 to 4.94, the SN-type nozzle shows larger impulse values than the CD-type nozzle. However, this does not automatically ensure better atomization for the SN-type nozzle than for the CD-type nozzle, since each nozzle can have a different geometrical efficiency that converts the atomization potential (somewhat similar to the impulse function) into the ultimate atomization (drop SMDs).

Drop Diameter Measurement and Data Analysis

The accuracy of the Malvern instruments was checked with a standard reticle [17]. The suggested calibration using the reticle estimated that the measurement uncertainties of spatially averaged SMDs ranged within ±3%. The radially resolved SMDs are expected to have somewhat larger uncertainties, since the tomographic reconstruction induces additional mathematical and numerical uncertainties. Other factors that can contribute to increasing the uncertainty include the drop asphericity, beam steering by the gas jets, and nonperfect correction of multiple scattering. The overall uncertainties of SMD measurements are estimated within ±7%.

The Rosin-Rammler two model parameters were modified to correct for the multiple scattering bias occurring for dense sprays with obscuration levels over 50% using the correction formulas of Felton et al. [18]. They developed a theoretical model to account for the multiple beam scattering effect on the SMD measurement biasing. Two correction

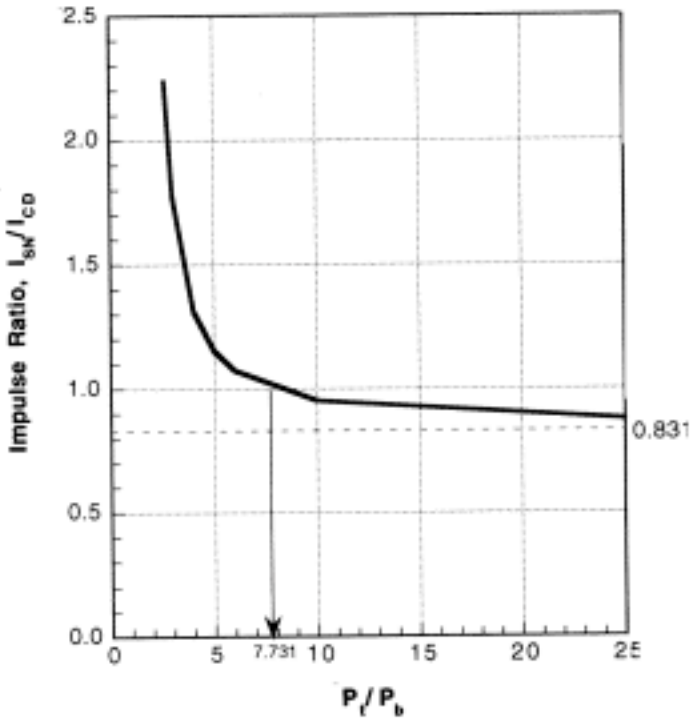

Fig. 4 Impulse ratio of SN-type nozzle to CD-type nozzle versus stagnation pressure normalized by back pressure.

formulas for the two model parameters as functions of the obscuration level was proposed and experimentally substantiated by using glass beads of known particle size ranges.

As we shall see, both nozzles develop sprays with minimal SMDs at the center and with increasing SMDs with the spray radius. The line-of-sight measured SMDs are larger than the radially resolved SMDs since the laser beam located at $r = r_o$ detects the signals coming from all the size bins distributed in $r_o \leq r \leq R$, where the drop SMDs are larger than that at $r = r_o$. In order to resolve this biasing to overestimated SMD data, a tomographic deconvolution technique converted the line-of-sight SMD data into radially resolved data. A variation of the onion-peeling method, which uses an Abel transform, was adopted assuming axisymmetric development of the sprays [11, 12].

RESULT AND DISCUSSION

Table 1 lists experimental conditions. Radial SMD distributions up to r = 55 mm were measured for three different liquid flow rates and at two different axial locations. Measurements were repeated for the two different type nozzles as the stagnation pressure varied as specified. The experimental results are presented in two steps: (1) local SMD

correlation based on a Buckingham-PI dimensional analysis, and (2) spatially averaged SMD correlation obtained from a modified energy model analysis.

Dimensional Analysis of Radially Resolved SMDs

When a specific liquid (water) is injected into a specified gas (nitrogen) jet environment, SMD is thought to be a function of the liquid tube diameter, axial and radial position coordinates with the origin located at the center of the liquid orifice exit, the liquid density, injection velocity, and mass flow rate, and the gas stagnation pressure which determines the gas jet velocity as well as its impulse. A functional form of SMD then gives

$$\text{SMD} = f(d_0, x, r, \rho_L, U_L, \dot{m}_L, p_t) \tag{5}$$

Equation (5) describes a parametric dependence of drop SMD when water is atomized by nitrogen gas jets injected through the two nozzle (SN and CD) configurations. A general form for SMD correlation must include additional parameters characterizing fluid property variations such as viscosity and surface tension coefficient.

The Buckingham-PI Theorem normalized the functional form of Eq. (5) giving five PI groups as

$$\pi_1 = \frac{\text{SMD}}{d_0} \qquad \pi_2 = \frac{x}{d_0} \qquad \pi_3 = \frac{r}{\cdot} \qquad \pi_4 = \frac{\dot{m}_L}{\rho_L U_L d_0^2} \qquad \pi_5 = \frac{p_t}{\rho_L U_L^2} \tag{6}$$

A functional relationship between the dimensionless parameters is established as

$$\frac{\text{SMD}}{d_0} = A\left(\frac{x}{d_0}\right)^B \left(\frac{r}{d_0}\right)^C \left(\frac{\dot{m}_L}{\sqrt{\rho_L p_b} \cdot d_0^2}\right)^D \left(\frac{p_t}{p_b}\right)^E \tag{7}$$

where the normalizing factors for $\dot{m}_L$ and p_t have been respectively substituted by $\sqrt{\rho_L p_b} \cdot d_o^2$ and p_b, since the liquid density ρ_L, the back pressure p_b, and the liquid delivery tube diameter d_o remain constant. Equation (7), therefore, gives a SMD correlation depending on selected parameters of x, r, $\dot{m}_L$, and p_t, for the case of water-nitrogen gas atomization. Coefficient A is determined differently for each type of nozzle, and the remaining constants B to E are determined from regression of the experimental data.

By using a linear least-squares statistical method with all of the experimental data for both the SN-type and the CD-type nozzles, an experimental correlation of drop SMD is obtained as:

$$\frac{\text{SMD}}{d_0} = A\left(\frac{x}{d_0}\right)^{-0.1367} \left(\frac{r}{d_0}\right)^{0.3742} \left(\frac{\dot{m}_L''}{\sqrt{\rho_L p_b}}\right)^{0.3588} \left(\frac{p_t}{p_b}\right)^{-0.7081} \tag{8}$$

where $\dot{m}_L''$ represents the injected liquid flux, mass flow rate in kilograms per unit time and per unit area of the orifice. Figure 5 compares the experimental results with the calculated values from the correlation given in Eq. (8). A statistical analysis of the correlation shows

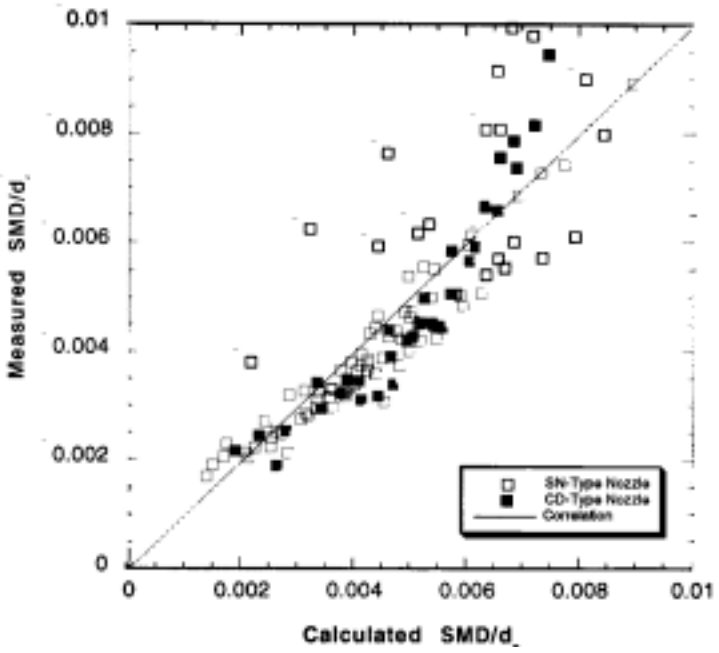

Fig. 5 Comparison of measured and calculated SMD data for both SN-type and CDtype nozzles.

over 90% confidence interval and a coefficient of multiple determination, R2, of 0.82. Most measured SMDs for both the SN- and CD-type nozzles show generally fair agreement with calculated values except for a few off-scattered data points. The correlation [Eq. (8)] shows a gradual decrease in SMD with increasing x, and SMD increases with increasing spray radius and with increasing liquid mass flux. The correlation shows the most significant dependence on p_t/p_b.

The geometric and physical constant A is determined as A = 0.0329 for the SN-type nozzle, and A = 0.0355 for the CD-type nozzle. The uncertainties associated with the individual measurements of x, r, $\dot{m}''_L$, and p_t, are estimated to ±0.01, ±0.02, ±0.01, and ±0.02, respectively. The SMD correlation uncertainty due to these individual uncertainties is calculated as ±0.017 by applying the standard uncertainty analysis suggested by Kline and McClintock [19]. A thing to note here is that the uncertainty contribution from p_t measurement is the most crucial to the SMD correlation uncertainty, since the magnitude of its exponent is the largest.

The SMD correlation coefficient A in Eq. (8) for the two nozzle types differs by only 7.5%, though the two nozzles develop quite different jet flow velocities under a same reservoir condition. For example, for p_t = 0.4 MPa and p_b = 0.1013 MPa, the nozzle exit velocity V_e = 603 m/s for the CD-type nozzle almost doubles the exit gas velocity of 322 m/s for the SN-type, yet the SMDs are not much different. We believe that this finding may suggest a distinction in assessing incompressible (M < 0.3) and compressible (M > 0.3) gas jets. For the case of an incompressible jet of constant density, the jet velocity directly

relates the other crucial properties for atomization, including the jet momentum, kinetic energy, and mass flow rate. For the case of compressible flow, the gas lowers its density with increasing jet velocity through an isentropic expansion, and the jet momentum and kinetic energy are hardly increased-with increasing velocity. Under the given example, the gas density at the nozzle exit $\rho_e = 0.634\ \rho_t$, for the underexpanded sonic jet of the SN-type nozzle and $\rho_e = 0.113\ \rho_t$ for the overexpanded CD-type jet. While the velocity is approximately doubled and the exit area is tripled for the CD-type nozzle, the gas density at the exit plane is reduced by a factor of 1/6. This also constitutes that the mass flow rate remains constant, since the stagnation pressure remains unchanged for the two nozzles. The stagnation pressure, instead of the jet exit velocity itself or other jet properties, seems to be a unique invariant in comparison of the two nozzles operating in compressible flow ranges. A detailed examination of individual parametric effects on the atomization follows.

Effect of Stagnation Pressure

Figure 6 shows radial SMD distributions for the SN-type nozzle depending on different stagnation pressures ranging from 0.2 to 0.5 MPa measured at x = 160 mm with Q = 200 ml/min. The symbols represent data and the curves show calculated SMD values based on Eq. (8). Increasing injection pressure enhanced the impulse and atomization characteristics, and the spray SMD decreases noticeably. The gas velocity slows down as r increases because its mixing with the entrained air is enhanced and the pressure reduces to the ambient level. This decreases the atomization potential or jet impulse near the spray boundary, and the SMD gradually increases in the radial direction. More rapid evaporation

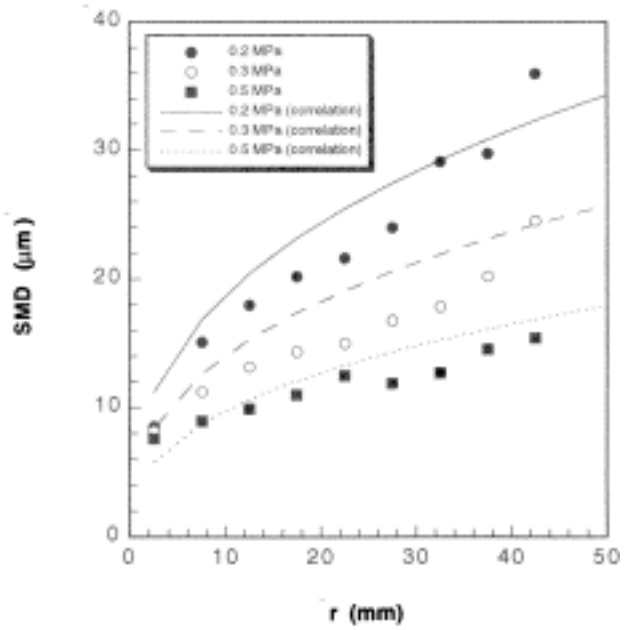

Fig. 6 Radial SMD distribution at x =160 mm under various gas injection ressure for SN-type nozzle with Q = 200 ml/min.

of smaller drops in the diffusive shear layer in the spray boundary contributes further to the SMD increase at large r.

Figure 7 presents similar results for the CD-type nozzle for stagnation pressures ranging from 0.25 to 0.4 MPa with all other injection parameters the same as those in Fig. 6. The agreement between the data and the correlation predictions is not as good when compared with the SN-type nozzle results in Fig. 6. These increased discrepancies between the data and calculations may be attributed to a larger and diverging nozzle exit configuration of the CD type, which could increase the uncertainties in its jet flow and atomization characteristics.

Effect of Liquid Flow Rate

Figure 8 shows radial SMD distributions measured at x = 160 mm for different liquid flow rates under 0.2 MPa gas injection from the SN-type nozzle. Since the stagnation pressure is constant for all cases, gas mass flow rate remains unchanged [Eq. (1)]. Increasing liquid flow rate under the same gas injection pressure thus reduces the gas-to-liquid mass ratio (GLR), and this decreasing GLR increases the drop SMD because of the reduction in shear energy per unit amount of the atomized liquid. The three liquid flow rates of 100, 200, and 300 ml/min, have equivalent GLRs of 2.516, 1.258, and 0.839, respectively (T_l = 300 K, R = 297 J/kg K, and γ = 1.4 for nitrogen). The correlation curves show fairly good agreement with the data other than a few scattered data points. A qualitatively similar effect of liquid flow rate is shown for the CD-type nozzle sprays, except that the overall SMDs are slightly larger than their counterparts for the SN-type nozzle sprays.

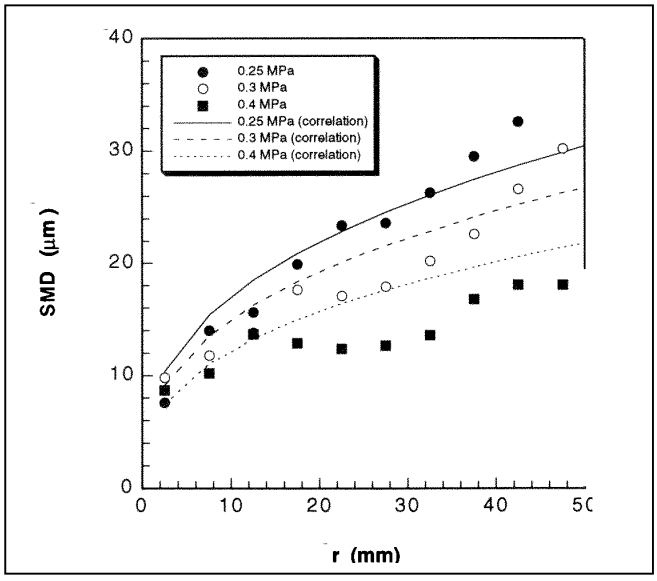

Fig. 7 Radial SMD distribution at x =160 mm under various gas injection pressure for CD-type nozzle with Q = 200 ml/min.

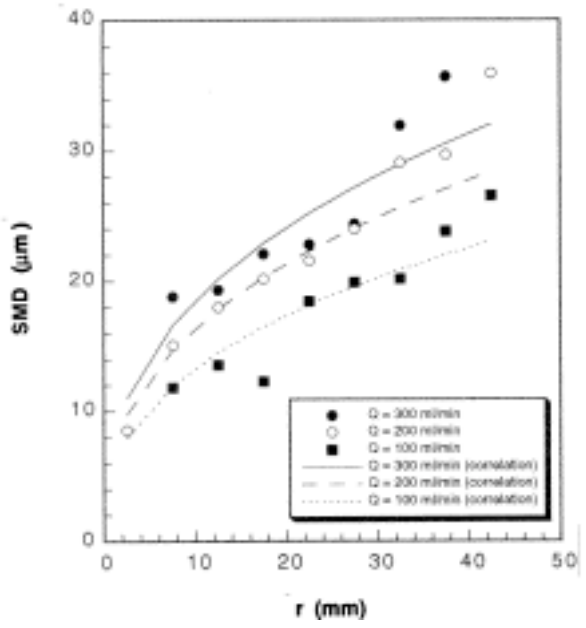

Fig. 8 Radial SMD distribution at x = 160 mm for different liquid flow rates under 0.2-MPa gas injection pressure from SN-type nozzle.

Effect of Axial Location

Figure 9 compares the atomization characteristics of the SN-type nozzle measured at 70 and 160 mm downstream of the nozzle exit. The liquid volume flow rate remained at 200 ml/min and the nozzle pressure was a constant 0.4 MPa. The measurement was extended to the radial location where the Malvern obscuration fell below 3% at each x location. Larger drops tended to move away from the centerline along with the spray because of their larger inertia-to-drag ratios. This depletion of larger drops can contribute to the gradual SMD decrease in the spray center, whereas the same depletion will contribute to the SMD increase at the spray edge along with increasing x. Additional factors in altering the spray SMD profile would be the preferential evaporation of smaller drops near the spray boundary and the increased drop coalition with the increasing travel or axial distance [20, 21]. Corresponding results for the CD-type nozzle sprays show a similar effect of the axial measurement location on the drop SMD distributions.

Spatially Averaged Drop SMDs

Spatially averaged SMDs are presented as functions of GLR accounting for the correct area weighting of each ring on the spray plane under the symmetric spray assumption in Fig. 10. The regular symbols with solid curves represent the SN-type nozzle, and the solid symbols with dashed curves represent the CD-type nozzle. A thing to note is that each type of nozzle does not significantly distinguish the average SMDs, and the SMDs

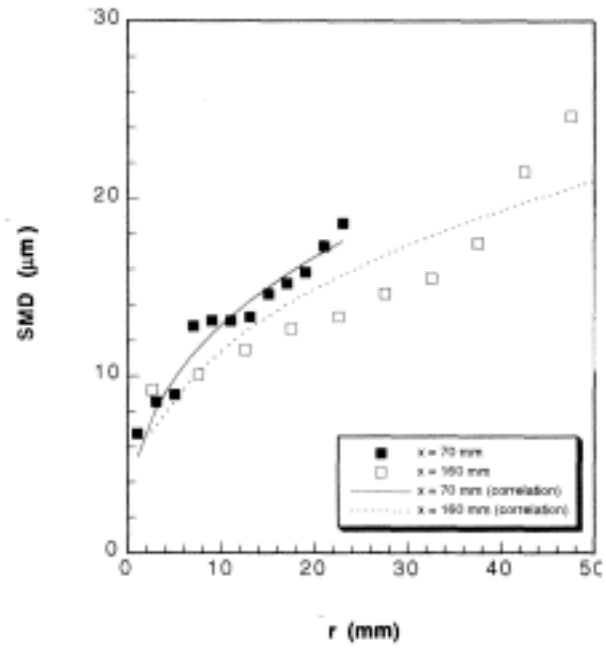

Fig. 9 Radial SMD distribution at two different axial locations for SN-type nozzle under 0.4 MPa and $\dot{Q}$ = 200 ml/min.

depend mainly on the liquid flow rate and GLR. The spatial distribution of local SMDs given in Eq. (8) shows a 7.5% difference in its geometric constant A between the two types of nozzles. Both the local and spatially averaged SMDs are determined primarily by the stagnation pressure rather than by the individual nozzle types.

Average SMDs show a rapid decrease with increasing GLR for a fixed liquid flow rate. This is because of the atomization energy increase of injected gas per atomized liquid fluid with increasing GLR. In contrast, SMD decreases for a given GLR with increasing liquid flow rate. The gas flow rate must increase proportionally with increasing liquid flow rate to maintain the same GLR. This increase of gas flow rate or, equivalently, the stagnation pressure, provides higher density-weighted relative jet velocity and higher nozzle exit pressure. In addition, doubling jet velocity, for example, will quadruple the kinetic energy. Both the impulse and kinetic energy will increase as a result of increasing stagnation pressure. This accelerated increase in the shearing energy transfer per unit liquid flow rate reduces the spray SMD when the liquid flow rate increases while the GLR is unchanged. This behavior coincides with the previous findings for the case of a plane two-dimensional nozzle [10].

Energy Model Analysis

The spatially averaged SMD data presented above were analyzed using a modified energy balance model originally suggested by Lefebvre [22]. Knoll and Sojka [13] used the model to analyze their experimental results obtained for air-assisted atomization by subsonic

air jets from a two-dimensional converging nozzle. The energy model correlated their measured average SMDs.

The energy model has been modified to apply to the present axisymmetric SN-type and CD-type nozzles and to account for both the underexpanded sonic and overexpanded supersonic gas jets, respectively. Applying the momentum balance to the control volume shown in Fig. 11, it follows that

$$\dot{m}_L U_L + \varepsilon \dot{m}_G U_G = (\dot{m}_L + \varepsilon \dot{m}_G) U \tag{9}$$

where the energy transfer efficiency, ε, represents the fraction of the total gas jets whose kinetic energy is entirely contributed to the liquid atomization. This also implies that the momentum exchange between the devoted gas of a fraction and injected liquid is completed in the control volume and they emerge from the exit plane with zero relative velocity. U denotes the spray penetration velocity at the exit plane.

The energy required for the atomization of a liquid jet can be expressed as the product of liquid surface tension coefficient and surface area change as [13]

$$E_L = \sigma_L (A_{L2} - A_{L1}) = \frac{2\sigma_L \dot{m}_L}{\rho_L} \left(\frac{3}{D} - \frac{2}{d_0} \right) \tag{10}$$

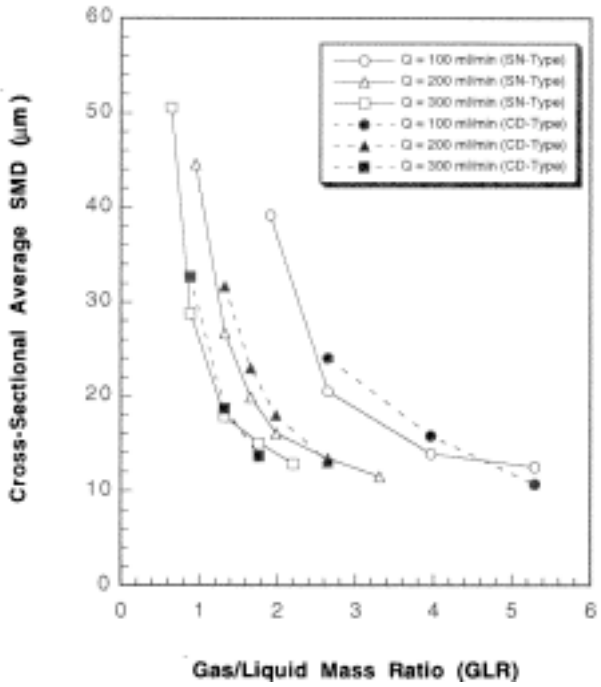

Fig. 10 Spatially averaged SMD versus gas/liquid mass ratio (GLR) for both SN-type and CD-type nozzles.

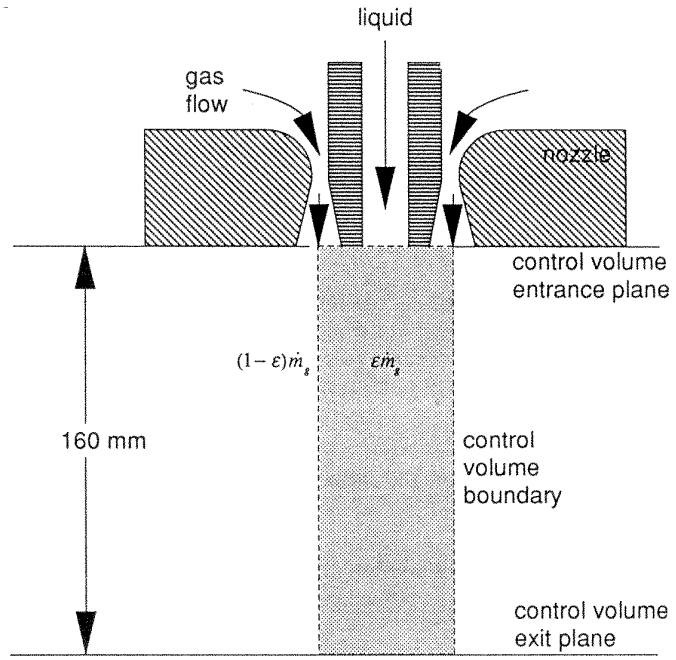

Fig. 11 Control volume for energy model.

where $\dot{m}_L''$ = $n\rho_L(\pi D^3/6)$, total surface area of atomized drops $A_{L2} = n\pi D^2$, and total surface area of liquid column before the breakup $A_{L1} = \pi d_o U_L$. d_o denotes the liquid orifice diameter and D indicates the atomized drop diameter.

Assuming one-dimensional flow and ignoring evaporation, the energy balance equation can be derived for the axisymmetric spray [17]:

$$\frac{\dot{m}_L U_L^2}{2} + \frac{\varepsilon \dot{m}_G U_G^2}{2} + \frac{4\sigma_L \dot{m}_L}{\rho_L d_0} = \frac{\dot{m}_L U^2}{2} + \frac{\varepsilon \dot{m}_G U^2}{2} + \frac{6\sigma_L \dot{m}_L}{\rho_L D} \tag{11}$$

where the gas and liquid drops are assumed to exit the control volume at an identical velocity U. Substituting Eq. (9) into Eq. (11) and replacing D with SMD, the average SMD for axisymmetric spray can be expressed as

$$\text{SMD} = \frac{12 d_0}{8 + \left\{\rho_L U_R^2 d_0/\sigma\left[1 + 1/(\varepsilon \cdot \text{GLR})\right]\right\}} = \frac{12 d_0}{8 + \left\{\text{We}_{d_0}/\left[1 + 1/(\varepsilon \cdot \text{GLR})\right]\right\}} \tag{12}$$

where the relative velocity U_R is defined as U_G subtracted by U_L. A thing to note is that the Weber number is defined with liquid density instead of more often use of gas density, i.e., $We_{do} = \rho_L U_R^2$ do/σ ranges from 2 x 10^4 to 1.25 x 10^5, where the relative gas velocity is estimated as 300 m/s and 750 m/s, respectively. The energy transfer efficiency, ε, should be known a priori to determine the spatially averaged drop SMD.

In the previous work using two-dimensional subsonic jets [13], the compressible flow feature was not considered and the primary factors known to affect £ were the gas velocity at the nozzle exit, gas-to-liquid mass ratio (GLR), and liquid viscosity. For the present case of underexpanded sonic or overexpanded supersonic jets, however, the normalized stagnation pressure, p_t/p_b, should be the dominant parameter that determines not only the nozzle exit behavior but also the compressible gas jet impulse as discussed in previous sections.

The relative gas velocity U_R in Eq. (12) is considered as a function of p_t/p_b and then the space-averaged SMD has a functional form of ε, GLR, and p_t/p_b. From a linear regression analysis of all the spatially averaged SMD data measured for both SN-type and CD-type nozzles against the calculated SMDs from Eq. (12), a single expression for ε is determined:

$$\varepsilon = \mathrm{GLR}^{-0.773}\left[2.374\times10^{-6}\left(\frac{p_t}{p_b}\right)^{3.773} - 3.585\times10^{-5}\left(\frac{p_t}{p_b}\right)^{2.773} + 1.543\times10^{-4}\left(\frac{p_t}{p_b}\right)1.773\right] \quad (13)$$

where ε shows a polynomial function of p_t/p_b. In the regression analysis, the relatively large inertial or impulse force of gas jets is assumed to override the viscosity effect that is concentrated near the spray shear boundary layers. The viscosity effect is represented by a viscous force acting on the injected liquid by the gas jet shear, i.e., $F_{VISCOUS} \cong \mu_L U_R d_o$. Thus, the ratio of the impulse or inertial force, I (Eq. 2), to the viscous force is given as

$$\frac{I}{F_{\text{viscous}}} \equiv \frac{\dot{m}_G V_e + (p_e - p_b)A_e}{\mu_L U_R d_0} \quad (14)$$

The ratio of $I/F_{Viscous}$ spans from 50 to 350 for the ranges of the tested parameters shown in Table 1. The impulse in Eq. (14) is calculated from Eq. (3) and Table 1 and the relative gas velocity with respect to the liquid velocity U_R is taken as a typical value of 500 m/s for the spray region near the nozzle exit.

For a given amount of liquid flow rate, GLR increases linearly with increasing gas flow rate expressed in Eq. (1), and Eq. (13) can now be expressed as

$$\varepsilon = \dot{m}_L^{0.773}\left\{2.374\times10^{-6}\left[\frac{A^* p_b}{\sqrt{RT_t}}\sqrt{\gamma}\left(\frac{\gamma+}{2}\right)^{(\gamma+1)/(2-2\gamma)}\right]^{-0.773}\right.$$
$$\left.\left(\frac{p_t}{p_b}\right)^3 - 1{:}\ 1\left(\frac{p_t}{p_b}\right)^2 + 65\left(\frac{p_t}{p_b}\right)\right]$$

or, equivalently,

$$\varepsilon = \dot{m}_L^{0.773}\ \ \mathrm{Const}\ \ \left[\left(\frac{p_t}{p_b}\right) - 15.10\left(\frac{p_t}{p_b}\right)^2 + 65\left(\frac{p_t}{p_b}\right)\right] \quad (15)$$

where the Const can be easily calculated with specified nozzle throat area, back pressure, stagnation temperature, and the gas specific heat ratio. The transfer efficiency shows a single correlation with the stagnation pressure for the two types of nozzles. This observation supports that the high-speed twin-fluid atomization is well characterized by the stagnation pressure as for the drop SMD correlation of Eq. (8).

Arbitrarily scaled energy transfer efficiency, $\varepsilon^* \equiv \varepsilon/\text{Const}$, is plotted as a function of the normalized stagnation pressure p_t/p_b for the three different liquid flow rates in Fig. 12. ε increases first and then decreases as p_t/p_b increases, and a local maximal energy transfer efficiency occurs at p_t/p_b of about 3.0. After a locally minimal value at $p_t/p_b \approx 7.0$, the energy transfer efficiency increases continuously with increasing p_t/p_b. This implies that the energy transfer is more efficient at higher p_t/p_b, when p_t/p_b is larger than 7.0, whereas a maximal energy transfer efficiency exists when p_t/p_b is less than 7.0. The transfer efficiency increases with increasing liquid flow rate under a given stagnation pressure. The range of the present p_t/p_b spans from 1.97 to 4.94.

Spatially averaged SMDs calculated from Eq. (12) in association with the transfer efficiency of Eq. (13) or (15) are compared with the measured SMDs in Fig. 13. The correlation shows excellent agreement with the data. Spatially averaged SMDs are well predicted by the modified energy model analysis, resulting in a single correlation with the stagnation pressure despite the nozzle types.

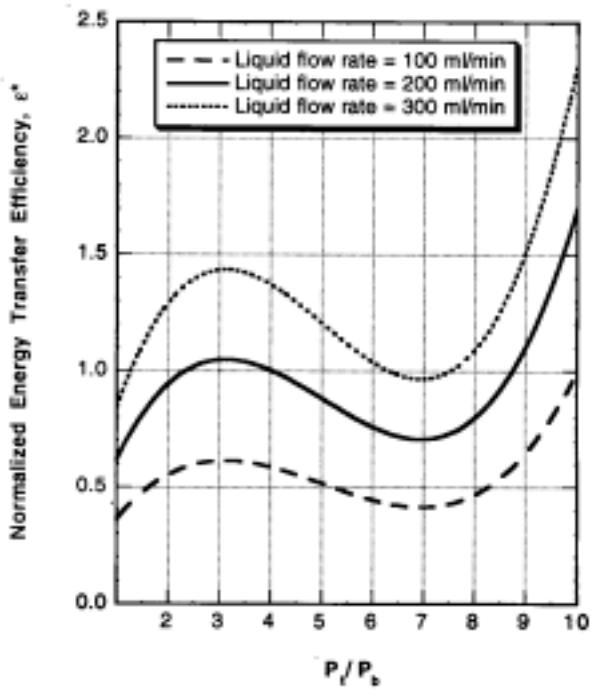

Fig. 12 Normalized energy transfer efficiency versus stagnation pressure for different liquid flow rates.

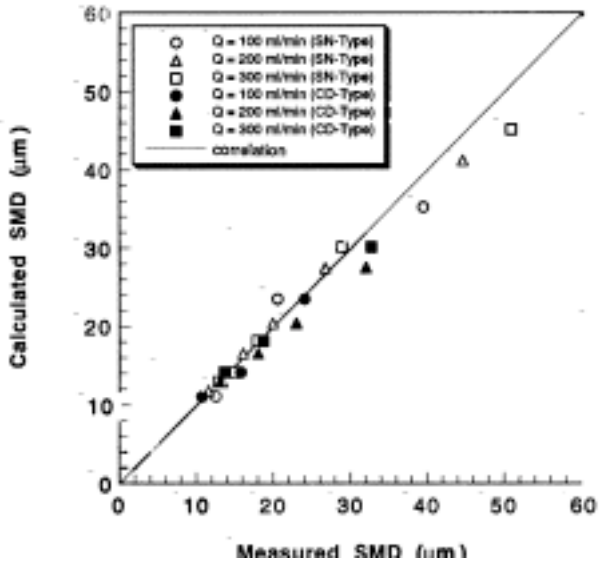

Fig. 13 Comparison of spatially averaged SMD data with the SMD calculations from the modified energy model.

CONCLUSIONS

Atomization characteristics of a single combination of twin-fluid (water and nitrogen gas) were investigated experimentally for two different types of gas injection nozzles: (1) a converging SN-type nozzle generating underexpanded sonic jets, and (2) a converging-diverging CD-type nozzle (AR = 3.0) generating overexpanded supersonic jets for the tested stagnation pressure range from 0.2 to 0.5 MPa. The Malvern diffraction technique with a Rosin-Rammler distribution model measured drop SMD data, and the measured line-of-sight data were converted into truly radial distribution via tomographic deconvolution based on a symmetric development of spray cross sections.

One major fording is that the atomization behavior is determined primarily by the stagnation pressure rather than by the type of nozzle tested. When the stagnation pressure is in the range where the SN-type nozzle is underexpanded and the CD-type nozzle is overexpanded, the supersonic jets generated from the CD-type nozzle do not necessarily improve atomization compared with the sonic jets from the SN-type nozzle.

The dimensional analysis shows a single form of the spatially resolved SMD distribution function for both nozzles, which shows SMD increasing with the spray radius and liquid mass flow rate and SMD decreasing with spray axis and stagnation pressure [Eq. (8)]. The modified energy model carried out for the spatially averaged SMDs showed a single correlation for both SN-type and CD-type nozzles [Eq. (12)]. The spatially averaged SMDs show a strong dependence on the gas-to-liquid mass ratio (GLR), the energy transfer efficiency [Eq. (13)], and the Weber number based on the nozzle dimension.

REFERENCES

1. K. Y. Kim and W. R. Marshall Jr., Drop-Size Distributions from Pneumatic Atomizers, AIChE J., vol. 17, no. 3, pp. 575-584, 1971.-
2. A. A. Rizkalla and A. H. Lefebvre, The Influence of Air and Liquid Properties on Airblast Atomization, J. Fluids Eng., Trans. ASME, pp. 316-320, 1975.
3. G. E. Lorenzetto and A. H. Lefebvre, Measurements of Drop Size on a Plain-Jet Airblast Atomizer, AIAA J., vol. 15, no. 7, pp. 1006-1010, 1977.
4. N. K. Rizk and A. H. Lefebvre, Spray Characteristics of Plain-Jet Airblast Atomizers, J. Eng. Gas Turbines Power, Trans. ASME, vol. 106, pp. 634-638, 1984.
5. A. R. Hanson, E. G. Domich, and H. S. Adams, Shock Tube Investigation of the Breakup of Drops by Air Blasts, Phys. Fluids, vol. 6, no. 8, pp. 1070-1080, 1963.
6. A. A. Ranger and J. A. Nicholls, Aerodynamic Shattering of Liquid Drops, AIAA J., vol. 7, no. 2, pp. 285-290, 1969.
7. A. A. Ranger and J. A. Nicholls, Atomization of Liquid Droplets in a Convective Gas Stream, Int. J. Heat Mass Transfer, vol. 15, pp. 1203-1211, 1972.
8. J. A. Schetz, P. W. Hewitt, and M. Situ, Transverse Jet Breakup and Atomization with Rapid Vaporization Along the Trajectory, AIAA J., vol. 23, no. 4, pp. 596-603, 1985.
9. A. Unal, Liquid Break-up in Gas Atomization of Fine Aluminum Powders, Metall. Trans. B, vol. 20B, pp. 619, 1989.
10. K. D. Kihm and N. Chigier, Effect of Shock Waves on Liquid Atomization of a Two-Dimensional Airblast Atomizer, Atomization and Sprays, vol. 1, no. 1, pp. 113-136, 1991.
11. L. G. Dodge, D. B. Rhodes, and R. D. Reitz, Drop-size Measurement Techniques for Sprays: Comparison of Malvern Laser-Diffraction and Aerometrics Phase/Doppler, AppL. Opt., vol. 26, no. 11, pp. 2144-2154, 1987.
12. D. C. Hammond, Jr., Deconvolution Technique for Line-of-Sight Optical Scattering Measurements in Axisymmetric Sprays, Appl. Opt., vol. 20, no. 3, pp. 493-499, 1981.
13. K. E. Knoll and P. E. Sojka, Flat-Sheet Twin-Fluid Atomization of High-Viscosity Fluids. Part I: Newtonian Liquids, Atomization and Sprays, vol. 2, no. 1, pp. 17-36, 1992.
14. A. H. Lefebvre, Twin-Fluid Atomization: Factors Influencing Mean Drop Size, Atomization and Sprays, vol. 2, no. 2, pp. 101-119, 1992.
15. J. E. A. John, Gas Dynamics, 2d ed., chap. 3, Allyn & Bacon, Boston, MA, 1984.
16. M. A. Saad, Compressible Fluid Flow, 2d ed., chap. 3, Prentice Hall, Englewood Cliffs, NJ, 1993.
17. B. K. Park, A Study on Spray Characteristics in Twin-Fluid Atomization and Solidification Process of Atomized Droplet, Ph.D. thesis, Department of Mechanical Engineering, Seoul National University, Seoul, Korea, 1994.
18. P. G. Felton, A. A. Hamidi, and A. K. Aigal, Measurement of Drop Size Distribution in Dense Sprays by Laser Diffraction, ICLASS-85, 1985.
19. S. J. Kline and F. A. McClintock, Describing Uncertainties in Single-Sample Experiments, Mech. Eng., vol. 75, no. 1, pp. 3-9, 1953.
20. K. D. Kihm, D. P. Terracina, S. E. Payne, and J. A. Caton, Synchronized Droplet Size Measurements for Coal-Water Slurry Sprays Generated from a High-Pressure Diesel Injection System, J. Inst. Energy, vol. 67, pp. 2-9, 1994.
21. K. D. Kihm, D. P. Terracina, and J. A. Caton, Spray Tip Droplet SMDs of Diesel Fuel (DF2) Intermittent High Pressure Sprays Compared with Coal-Water Slurry (CWS) Sprays, J. Inst. Energy, vol. 68, pp. 574, 1995.
22. A. H. Lefebvre, Energy Considerations in Twin-Fluid Atomization, ASME J. Eng. Gas Turbines Power, vol. 114, no. 1, pp. 89-96, 1992.